J Mater Sci: Mater Electron (2010) 21:1299–1307
DOI 10.1007/s10854-010-0066-2

# Role of substrate temperature on the structural, optoelectronic and morphological properties of (400) oriented indium tin oxide thin films deposited using RF sputtering technique

**V. Malathy · S. Sivaranjani · V. S. Vidhya · T. Balasubramanian · J. Joseph Prince · C. Sanjeeviraja · M. Jayachandran**

Received: 9 December 2009 / Accepted: 18 January 2010 / Published online: 2 February 2010
© Springer Science+Business Media, LLC 2010

**Abstract** RF sputtering process has been used to deposit highly transparent and conducting films of tin-doped indium oxide onto quartz substrates keeping the RF power constant at 250 W. The electrical, optical and structural properties have been investigated as a function of substrate temperature. XRD has shown that deposited films are polycrystalline and have (400) preferred orientation. Indium tin oxide layers with low resistivity values and high transmittance in the visible region have been deposited. Detailed Analyses based on X-ray diffraction, optical and electrical results are attempted to gain more insight into the factors that are governed by the influence of varying substrate temperature in this investigation. AFM pictures showed uniform surface morphology with very low surface roughness values. It has been observed that ITO films deposited in this study, keeping the substrate temperature at 150 °C, can provide the required optimum electrical and optical properties rendering them useful for developing many optoelectronic devices at a moderate temperature.

V. Malathy · T. Balasubramanian
Department of Physics, National Institute of Technology, Trichy 620 015, India

S. Sivaranjani · J. J. Prince
Department of Physics, Anna University, Trichy 620 024, India

V. S. Vidhya · M. Jayachandran (✉)
ECMS Division, Central Electrochemical Research Institute, Karaikudi 630 006, India
e-mail: mjayam54@yahoo.com

C. Sanjeeviraja
Department of Physics, Alagappa University, Karaikudi 630 003, India

## 1 Introduction

Semiconductor thin films exhibiting simultaneously high electrical conductivity and optical transparency are of major technical importance, for instance in solar cells, flat panel displays, and electrochromic devices [1]. The required combination of properties can be realized by degenerate doping of wide band gap oxide semiconductors such as $In_2O_3$, $SnO_2$, or ZnO [2]. Among these, tin-doped indium oxide, also called indium-tin oxide (ITO), shows the highest electrical conductivity, which in combination with its high optical transmittance has projected it as the most widely used Transparent Conductive Oxide (TCO) in developing many optoelectronic devices [3]. TCO films are produced in vacuum or gas phase based methods, such as sputtering or chemical vapour deposition [2]. Due to the high crystallinity and compactness of the resulting thin films, excellent electrical conductivities can be achieved under the optimized preparative conditions.

Indium tin oxide films have been deposited containing $Sn^{4+}$ ions hosted in the $In_2O_3$ structure with concentrations varying up to 15% [4]. ITO is a highly degenerate n-type semiconductor with a wide band gap (3.5–4.3 eV), having very low electrical resistivity of about $10^{-4}$ Ω cm making it easy to be interfaced with electronic circuits and simultaneously shows high transmission in the visible and near infrared (NIR) regions of the electromagnetic spectrum [5]. Its low resistivity results from either the non-stoichiometry produced by oxygen deficiency or the incorporation of tin as tetravalent dopant or from both [6]. Moreover, ITO exhibits excellent substrate adherence, hardness, and chemical inertness. These distinct physico-chemical properties of ITO is widely used in optoelectronic devices such as solar cells, flat panel displays, electrochromic devices, anti-reflection coatings and gas sensors [5]. ITO thin films

can be prepared by various techniques such as spray pyrolysis [7], pulsed laser deposition [8], sol–gel method [9], magnetron sputtering [10], electron beam evaporation [11], chemical vapor deposition [2]. Among these techniques, sputtering deposition is unique one which achieves the deposition of a variety of materials without heating the source materials.

Many authors reported that the ITO films deposited at room temperatures are generally of amorphous structure [12]. In particular, substrate temperature is one of the most important key parameters to prepare highly conductive ITO films [13]. Further, developing efficient or improved organic light emitting devices (OLED) and organic solar cells need relatively lower process temperature for making the constituent ITO and organic coatings [14]. ITO films with low resistivity and high transmittance were deposited by negatively biased DC magnetron sputtering process in which the attracted cations are believed to give addition energy favoring formation of crystalline films at room temperature obviating higher substrate temperature usage [15]. Hence, we have used a high RF power of 250 W in the present study so that the substrate temperature can be lowered and highly oriented ITO films with good transparency as well as low resistivity can be obtained. In this paper we report the structural, morphological, electrical and optical studies of ITO thin films deposited by RF magnetron sputtering technique using 250 W power on quartz substrates kept at different temperatures.

## 2 Experimental

Indium-tin oxide films were deposited on quartz substrates at 250 W using a 13.56 MHz radio frequency magnetron sputtering system with 99.99% pure tin doped indium oxide (Indium 90%: Tin 10%) ceramic target. The base pressure of the deposition chamber was $10^{-6}$ torr and the working pressure was kept at $5 \times 10^{-3}$ torr under pure argon ambient. Sputtering was carried out by keeping the target to substrate distance constant at about 8 cm through out the experiment. The substrate temperature was varied between 50 and 250 °C in steps of 50 °C and the deposition was carried out for different durations from 5 to 30 min so as to maintain the thickness of the films in the range 400–450 nm. The quartz substrates were first cleaned by a detergent, washed with distilled water, kept in freshly prepared hot chromic acid for 1 h, again thoroughly cleaned with distilled water and finally subjected to ultrasonic cleaning for 1 h. Film thickness was measured by the Stylus Profilometer (Mitutoyo). The optical transmittance measurements were made in the wavelength range 300–2400 nm using a Hitachi-330 UV–Vis–NIR spectrophotometer. X-ray diffraction (XRD) measurements were carried out with X'pert Pro PANalytical-3040 using CuK$\alpha$ radiation ($\lambda = 1.5406$ Å) to study the structural properties of the films. Electrical properties were measured by the four probe method with a Four probe set up model DEP-02 (Scientific Equipment) DC power supply. Hall mobility and carrier concentration were calculated from the Hall voltage measured by VanderPauw method with a Ecopia HMS 3000 Hall constant measurement system. The surface morphology and roughness of the films were analyzed using a Nanoscope E-3138j AFM/STM Atomic force microscope (AFM).

## 3 Results and discussions

### 3.1 Crystalline orientation and texture

The X-ray diffraction patterns of ITO film deposited at different temperature are shown in Fig. 1. It is clear from the figure that the predominant orientation is (400) for all the films. It is also seen that the intensity of the (400) peak increases with increasing substrate temperature up to 150 °C and then decreases. It is observed that the (222) peak and (440) peak coexist with (400) peak for all the films deposited at temperatures 50–250 °C which clearly correspond to the formation of $In_2O_3$ cubic structure with highly oriented crystalline nature.

From Fig. 1, the XRD intensities of (222) and (400) peaks $I_{222}$ and $I_{400}$ respectively were obtained and the

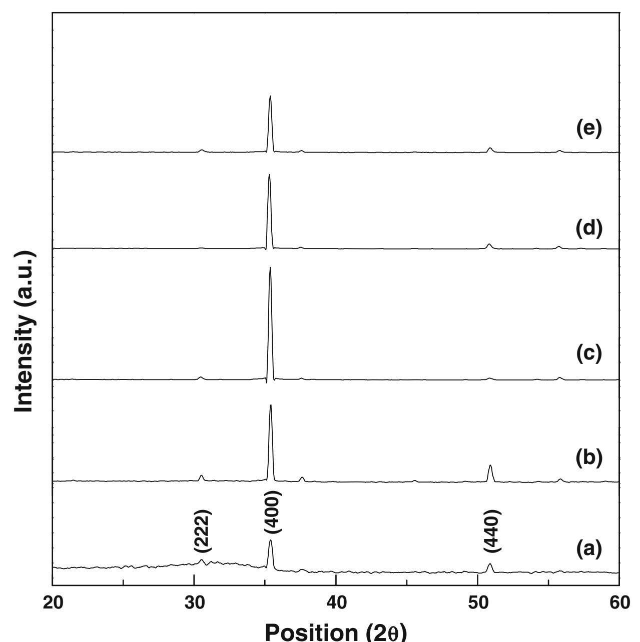


**Fig. 1** X-ray diffraction patterns for ITO films deposited at different substrate temperatures: (*a*) 50, (*b*) 100, (*c*) 150, (*d*) 200 and (*e*) 250 °C

variation of $I_{222}$, $I_{400}$ and $I_{222} + I_{400}$ values are shown in Fig. 2. The behavior of XRD peak intensities shows two common and important observations: (1) the continuous increase up to the substrate temperature 150 °C (2) a continuous decrease in the 200–250 °C region. This result is in accordance with the observed orientation behavior for the ITO films prepared by sputtering techniques. It is reported that the preferred orientation of ITO films depends on the adatom mobility [16] and the highly energetic (~10 eV) sputtered adatom which favors the films growth along some simple crystal planes like (100) [17]. In the present study, sputtering is carried out at a high RF power 250 W which generally produces sputter adatoms with high energy. The elevated substrate temperatures (150–250 °C) employed also may increase the adatom mobility. Due to these effects, all the deposited ITO films showed preferred orientation along (400) plane only. Similar result has been reported for ITO films deposited by DC magnetron sputtering technique [18] where the intensity of (400) plane was found to increase with substrate temperature. Further, another important reason for (400) preferential orientation in ITO films is that the concentration of oxygen vacancies during high power as well as high temperature sputtering is high due to the reduced sticking coefficient of oxygen at high temperatures [19].

### 3.2 Net lattice distortion and microstrain

The net lattice distortion ($\Delta d/d_{\mathrm{hkl}}$) can be expressed as:

$$\Delta d/d_{\mathrm{hkl}} = (d_{\mathrm{exp}} - d_{\mathrm{hkl}})/d_{\mathrm{hkl}} \tag{1}$$

where $d_{\mathrm{exp}}$ is the distance between the lattice planes which is derived from the experimental peak position by means of the Bragg formula and $d_{\mathrm{hkl}}$ is the value for the unstrained crystalline film.

The XRD line broadening in polycrystalline materials can be due to a finite grain size or microstrain. The statistical microstrain ε in the films is correlated with the XRD line broadening $\Delta(2\theta)$ by [20]:

$$\Delta(2\theta) = 2\tan(\theta)\varepsilon \tag{2}$$

In Fig. 3, the variation of microstrain and lattice distortion is displayed versus the substrate temperature for the (400) orientation for present in all the sputtered ITO films. The lattice distortion and microstrain under different substrate temperatures are quite low and showing the same trend of decreasing up to 150 °C and then increasing. ITO films deposited at 150 °C show the minimum lattice distortion and microstrain. This phenomenon can be interpreted in terms of the different discharge mechanisms when larger RF power, here 250 W, is used. The largest part of the energetic particles (bombarding energetic ions) has its origin in the plasma in front of the substrate. Therefore, the energy flux in the growing film is not influenced in such cases [21] which develop the same magnitude of microstrain and distortion in the crystal lattice of ITO films. It is also reported that such a high energy ion bombardment on growing ITO films may

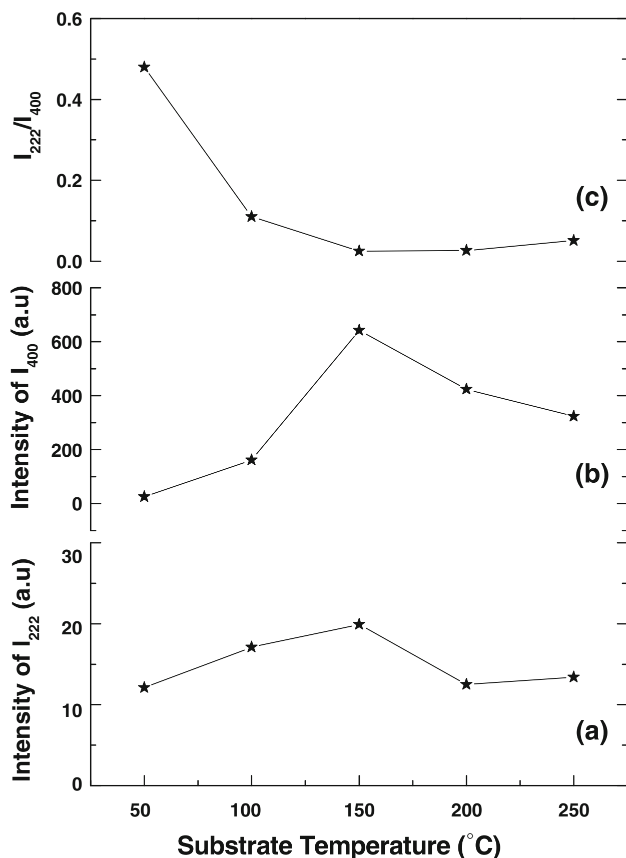


**Fig. 2** Variation of (*a*) the XRD intensities of (222) plane, (*b*) (400) plane and (c) the ratio of the peak intensities ($I_{222}/I_{400}$)

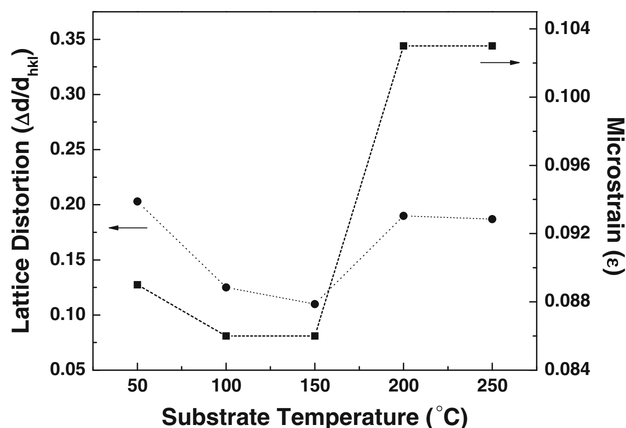


**Fig. 3** The lattice distortion and the microstrain variation for the sputtered ITO films deposited at different temperatures

damage the lattice structure effecting a lattice distortion [22].

### 3.3 Correlation between the electrical properties and microstructure of ITO films

Figure 4 shows the variations in electrical properties, resistivity ($\rho$), carrier concentration ($N$) and mobility ($\mu$) of ITO films prepared by RF sputtering at 250 W under various substrate temperatures. The lowest resistivity is obtained at 150 °C and the corresponding value is $2.2 \times 10^{-3}$ Ω cm. The carrier concentration reaches a maximum value $3.4 \times 10^{20}$ cm$^{-3}$ at 150 °C and then starts decreasing whereas the carrier mobility reaches its highest value of 12.1 cm$^2$/V s at 150 °C and then exhibits a decreasing trend.

Further, XRD provides interesting information that reveals substantial correlation between the carrier mobility and microstructure. The XRD peaks of all ITO samples correspond well to $In_2O_3$ structure by comparing them with the standard XRD data [23] and no peaks corresponding to other phases like Sn, SnO, $SnO_2$ are observed which reveals that the tin atoms were doped substitutionally in the $In_2O_3$ crystal lattice. Since (400) is the XRD peak with maximum intensity for all the ITO films, its full width at half maximum (FWHM) $\beta$ is used in Scherrer formula,

$$D = \frac{0.9\lambda}{\beta \cos\theta} \tag{3}$$

to calculate the grain size ($D$) of the deposited ITO films. Moreover, ITO films with such high carrier concentration, behave like degenerate semiconductors and the mean free path L of conduction electron can be calculated using the model of Free electron Fermi gas [24],

$$L = \frac{h}{2q}\left(\frac{3N}{\pi}\right)^{1/3}\mu \tag{4}$$

The grain size and mean free path values calculated at different temperature are shown in Fig. 5a. The variation in grain size is less appreciable and it varies nominally from about 26.1 to 29.5 nm when the temperature was varied from 50 to 250 °C, respectively. But the grain size reached a maximum of about 45.4 nm at 150 °C. The mean free path for electrons in these films varies between 0.65 and 1.32 nm. Comparison of $D$ and $L$ values shows that the grain size is greater than the mean free path of electrons in all the ITO films. It reveals that grain boundary scattering plays a minor role on the carrier mobility in these films and

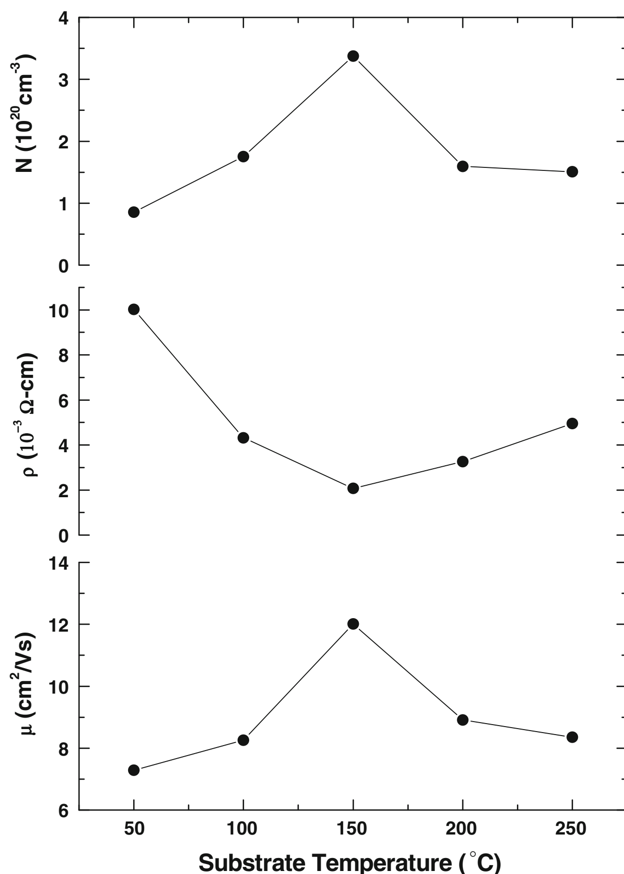


**Fig. 4** Resistivity ($\rho$), Carrier concentration ($N$) and Hall mobility ($\mu$) of ITO films deposited at different temperatures

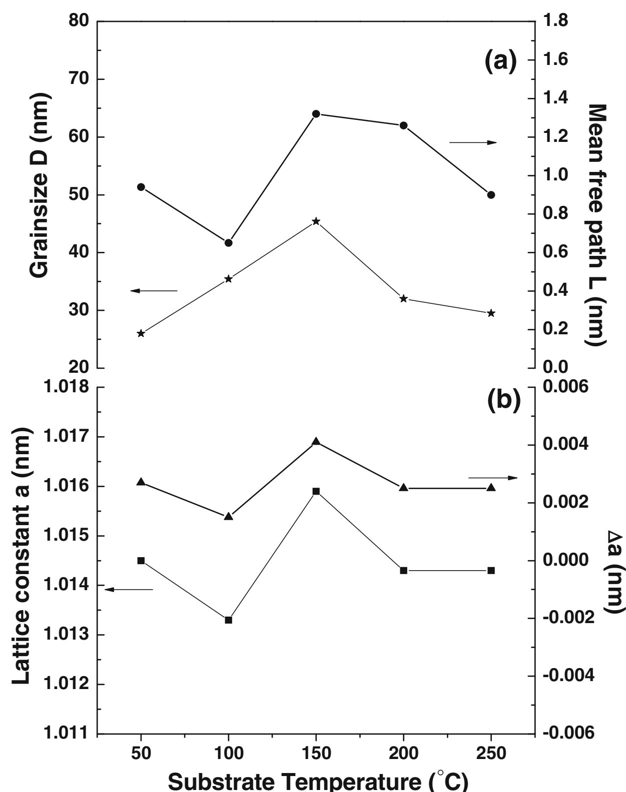


**Fig. 5** Dependence of ($a$) Grain size ($D$) and Mean free path ($L$), and ($b$) Lattice constant ($a$) and $\Delta a$ with substrate temperatures

impurity scattering may be considered to be dominant. Also, the position of (400) peak $(2\theta)_{400}$ is used to calculate the lattice constant 'a' of each ITO film and the deviation $\Delta a$ from the standard value of $In_2O_3$ (1.0118 nm) is obtained as $\Delta a = (a - 1.0118)$ nm. Figure 5b shows the dependence of 'a' and 'Δa' values with substrate temperature. A negative value of $\Delta a$ means lattice contraction and a positive value means lattice expansion.

Frank and Kostlin [25] found that at the same and high doping level, the lattice constant of oxidised ITO film is smaller than that of reduced ITO film. The lattice constant change indicated by $\Delta a$ value of our samples shows that all the samples have positive $\Delta a$ as seen from Fig. 5b. Introduction of Sn into the crystal lattice [26] and the incorporation of oxygen into the ITO film [27] would lead to an enlargement of the lattice constant to some extent. Such a positive $\Delta a$ value indicates that the films are in more reduced state and the films deposited at 150 °C, possess greater value of $\Delta a$ (=+0.0041 nm), which can have higher electron mobility [28] and grains highly oriented along (400) plane. Further, high sputtering energy, high deposition temperature during sputtering [29], or using oxygen-free electron cyclotron resonance sputtering [30] has been observed to be favourable for the growth of (400) oriented ITO films, which results support the formation of highly (400) oriented ITO films prepared with 250 W RF power, substrate temperature 150 °C and oxygen free argon atmosphere in the represent study.

### 3.4 Variation of optical properties with temperature

Figure 6 shows the transmission spectra recorded for ITO films deposited at various temperatures (50, 150 and 250 °C). These films show good transmittance properties of about 80–90% in the visible and near-infrared regions. The average transmittance calculated in the wavelength region from 400 to 800 nm is higher than 85% which varies for the ITO films deposited at different temperatures. It is obvious that the transmittance in the visible region is determined by the crystalline nature and surface morphology. A gradual shift of the absorption edge towards higher energy with increasing substrate temperature is observed.

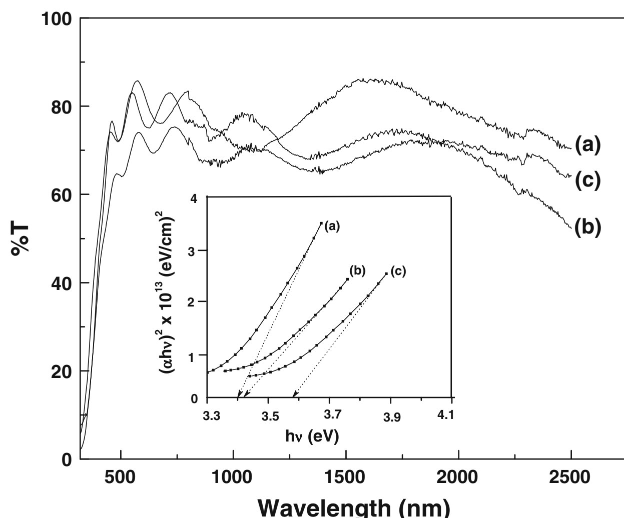


**Fig. 6** Transmittance spectra of ITO films deposited at temperatures (*a*) 50, (*b*) 150 and (*c*) 250 °C. *Inset* gives the $(\alpha h\nu)^2$ vs. $h\nu$ curves

The optical absorption coefficient ($\alpha$) as a function of transmittance ($T$) and reflectance ($R$) is given by the following expression that considers multiple internal reflections [31]:

$$\alpha = \frac{1}{t}\ln\left[\frac{(1-R^2)}{2T} + \left\{\left[\frac{(1-R^2)}{2T}\right]^2 + R^2\right\}^{1/2}\right] \tag{5}$$

where $t$ is the thickness of the ITO film. From the transmittance spectra is the UV region, if reflection is neglected, the absorption coefficient can be calculated from the following equation obtained from simplifying the Eq. 5:

$$\alpha = \frac{1}{t}\ln\left(\frac{1}{T}\right) \tag{6}$$

The optical band gap of ITO films can be determined from the analysis of the spectral dependence of the absorption near the fundamental absorption edge using the transmittance spectra. In this absorption region the absorption coefficient $\alpha$ is represented by the Tauc relation,

$$\alpha h\nu = A(h\nu - E_g)^m \tag{7}$$

where $A$ is a parameter that depends on the transition probability, $h\nu$ is the photon energy, $E_g$ is the band gap and $m$ is an exponent, which assumes the values 1/2, 2, 3/2, and 3 for allowed direct, allowed indirect, forbidden direct and forbidden indirect optical transitions, respectively [32].

For the ITO films deposited at different substrate temperatures, the band gaps were obtained by plotting $(\alpha h\nu)^2$ vs. $h\nu$ and extrapolating the straight line portion at high energies of this plot to the energy ($x$-axis) axis. From the intercept of the linear portion of these plots, optical band gap ($E_g$) values obtained are 3.40, 3.44, 3.58, 3.49, 3.42 eV for the ITO films deposited at 50, 100, 150, 200 and 250 °C, respectively. The representative $(\alpha h\nu)^2$ vs. $h\nu$ curves for ITO films deposited at 50, 150 and 250 °C are shown in the inset of Fig. 6. The observed band gap values are in good agreement with the reported value of about 3.41 eV for the ITO films electron beam evaporated at 300 °C [33].

When the substrate temperature is increased from 50 to 150 °C, the band gap increases which is caused by the increase of carrier concentration and filling of the

electronic states near the bottom of conduction band of ITO lattice. From the XRD results, it is observed that the grain size increases when the substrate temperature is increased from 50 to 150 °C which reveals that the free electrons are trapped at the grain boundaries and grain boundary scattering becomes dominant. This is also supported by the increasing carrier concentration and decreasing resistivity up to the deposition temperature region 50–150 °C as seen in Fig. 4. When the grain sizes are larger, the density of grain boundary decreases and consequently the number of trapped carriers is less which makes the availability of higher amount of carriers for conduction. Such a variation in carrier concentration leads to a modification in the optical band gap of degenerate semiconductor films which is related to the Burstein–Moss effect [1] and represented as:

$$E_g - E_{go} = \Delta E_{gBM} = \frac{h}{2m^*}(3\pi^2 n_e)^{2/3} \tag{8}$$

where $E_{go}$ is the intrinsic (undoped) band gap, $m^*$ is the electron effective mass. The increase in band gap and decrease in resistivity of ITO films may be due to $Sn^{4+}$ doping or oxygen vacancies which are acting as donors [34].

It can be suggested that the concentration of electrically active Sn atoms and oxygen vacancies increase when the substrate temperature is increased to 150 °C keeping the RF power high at 250 W for the deposition of ITO films in the present study. The decrease of band gap for the ITO films deposited at 200 and 250 °C may be attributed to oxygen deficiency which is also Burstein–Moss shift. This can be due to the fact that the carrier concentration of these ITO films gets reduced because of the creation of acceptor type non-stoichiometric defects produced at these deposition conditions (higher temperature, high RF power), which may be acting as compensation centres.

Refractive index and extinction coefficient values of ITO films in the wavelength range 400–1000 nm were calculated from the interference patterns of transmission spectra. The refractive index of the prepared ITO thin films was calculated from the measured transmittance spectrum. The evaluation method used in this work is based on the analysis of the transmittance spectrum of a weakly absorbing film deposited on a non-absorbing substrate [35, 36]. The refractive index $n(\lambda)$ over the spectral range is calculated by using the envelopes that are fitted to the measured extrema and minima as:

$$n(\lambda) = \sqrt{S + \sqrt{S^2 - n_0^2(\lambda) n_s^2(\lambda)}} \tag{9}$$

$$S = \frac{1}{2}\left(n_0^2(\lambda) + n_s^2(\lambda)\right) + 2n_0 n_s \frac{T_{max}(\lambda) - T_{min}(\lambda)}{T_{max}(\lambda) \times T_{min}(\lambda)} \tag{10}$$

where $n_0$ is the refractive index of air, $n_s$ is the refractive index of the substrate, $T_{max}$ is the maximum envelope and $T_{min}$ is the minimum envelope.

The extinction coefficient, $k$ was obtained by the relation,

$$k = \lambda\alpha/4\pi \tag{11}$$

where, $\lambda$ is the wavelength at which $T_{max}$ and $T_{min}$ are derived [37]. Figure 7 shows the variation of refractive index and extinction coefficient with wavelength for the ITO film deposited at 150 °C with RF power 250 W. It shows a high refractive index value of 1.95 at 550 nm which agrees well with the values of 1.8–2.1 reported for highly conducting ITO films [38, 39] and also with the reported value of 1.86 for the ITO films deposited by reactive RF magnetron sputtering [40]. The average extinction coefficient value is about 0.07. It confirms the formation of highly compact, void free and fully crystallized structure of the ITO films deposited at 150 °C with RF power held at 250 W.

The two important optoelectronic properties, high transmittance and high conductivity ($1/\rho$), of the ITO films do not co-exist with each other. There is an intrinsic requirement to reach a trade-off between these two properties for a specific application. The figure of merit, $\phi_{TC}$, is a parameter used to evaluate the quality of transparent conducting oxide (TCO) films like ITO and is defined by Haacke [41] as

$$\phi_{TC} = \frac{T_{av}^{10}}{R_s} \tag{12}$$

where $T_{av}$ is the computed average transmittance percentage in the wavelength range 400–800 nm and $R_s$ is the sheet resistance in Ω/□. The $\phi_{TC}$ reaches a maximum of $5.2 \times 10^{-3}\ \Omega^{-1}$ and a minimum of $R_s = 12.4$ Ω/□ for the ITO films deposited at 150 °C. Figure 8 shows the changes

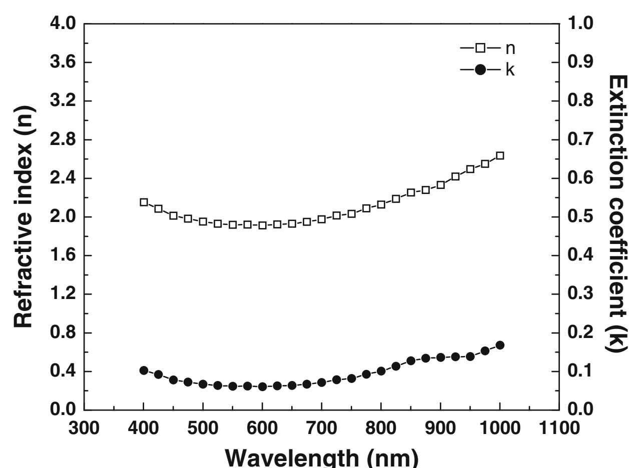


**Fig. 7** The variation of refractive index and extinction coefficient with wavelength for the film deposited at 150 °C

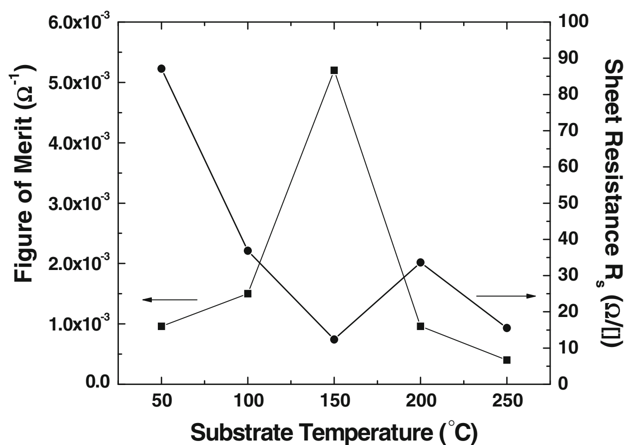


**Fig. 8** Variation of Figure of merit and sheet resistance of ITO films with substrate temperature

in $R_s$ and $\phi_{TC}$ with temperature. This is comparable with the reported values of 11.2–17.8 $\times$ $10^{-3}$ $\Omega^{-1}$ for the ITO films deposited by bias magnetron RF sputtering technique [42]. Also in good agreement with the $\phi_{TC}$ values of 0.3 $\times$ $10^{-3}$ and 6.4 $\times$ $10^{-3}$ $\Omega^{-1}$ for the 10% Sn doped ITO single layer and multilayer films respectively deposited without intentional heating on polycarbonate substrate [43]. Based on the fact that higher the $\phi_{TC}$ value, better the optoelectronic quality of TCO films [44], it shows that ITO films deposited at 150 °C with 250 W RF power have better optoelectronic properties than other films.

### 3.5 Surface morphology

Figure 9a–c presents the AFM surface morphology (3D images) and surface profile of ITO films deposited on

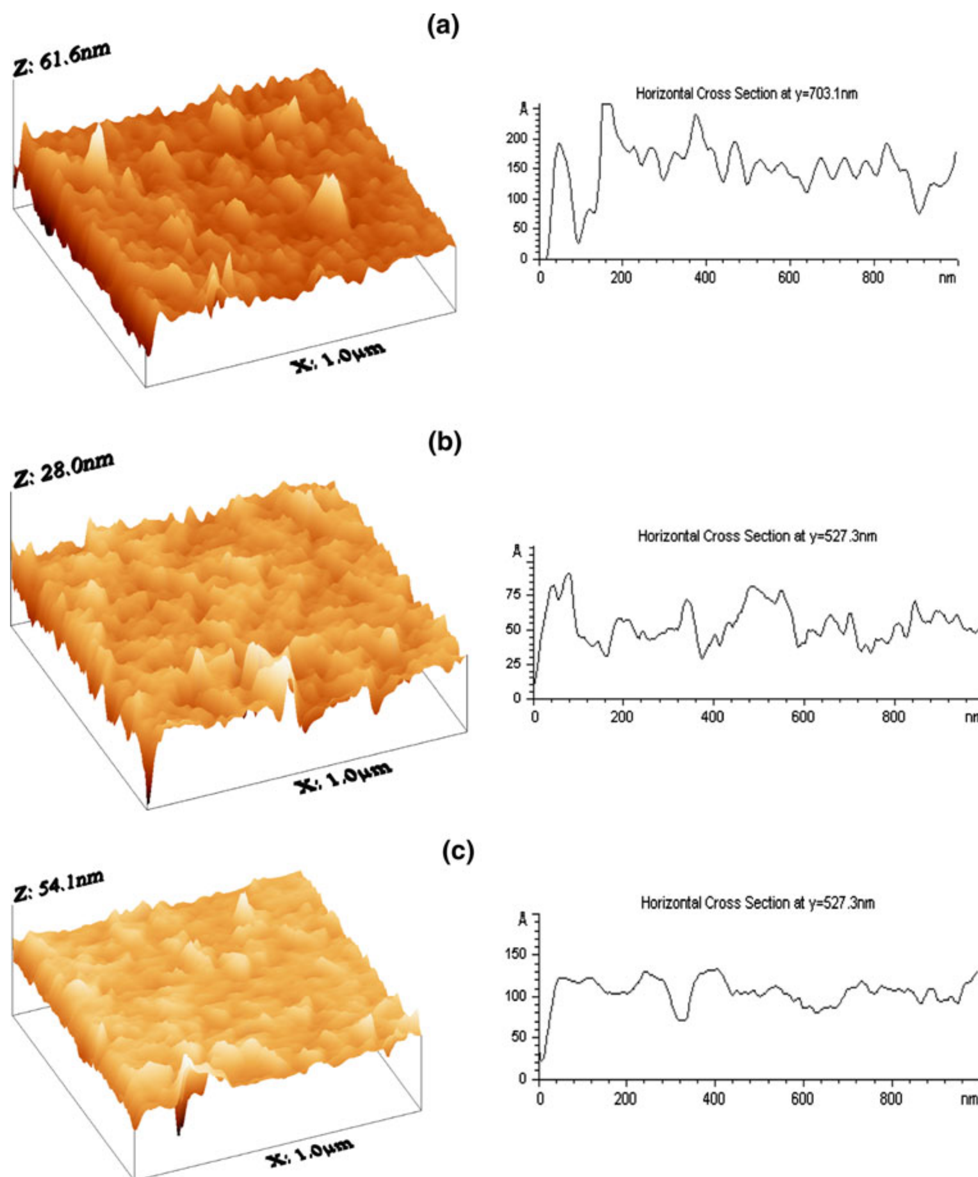


**Fig. 9** AFM pictures and corresponding surface profiles of ITO films deposited at **a** 50, **b** 150 and **c** 250 °C

quartz substrates at temperatures 50, 150 and 250 °C, respectively. The films were deposited without oxygen inclusion at high RF power 250 W and the morphology of the films shows significant variation with temperature. The roughness values were obtained from an area of 1 μm × 1 μm wherein a closure look at the surface deviation between the grains or clusters of grains is possible. The Root-Mean-Square value of roughness ($R_{rms}$, nm), the difference in height between the highest and lowest points on the surface height deviations measured from the mean plane derived as peak-to-valley roughness ($h_{p\text{-}v}$, nm) and the average differences of heights ($h_{av}$, nm) were derived from Fig. 9a–c. These values ($R_{rms}$, $h_{p\text{-}v}$, $h_{av}$) for the ITO films deposited at 50, 150 and 250 °C, respectively are: (1) 3.83, 61.59, 29.85 nm, (2) 1.77, 28.00, 14.12 nm, (3) 2.86, 54.14, 35.87 nm. The minimum surface roughness value is observed for the ITO films deposited at 150 °C which shows more uniform surface morphology with clusters of nano grains than the other films deposited at 50 and 250 °C. However, all the ITO films show nano-scale morphology with compact, uniform and pin-hole free surface.

## 4 Conclusion

The RF magnetron sputtering technique has been used to deposit ITO thin films on quartz substrates at 250 W with different substrate temperatures in argon ambient without oxygen. Role of different substrate temperatures during deposition on the structural, optoelectronic and morphological properties have been studied in detail. XRD results of the films confirm cubic structure with (400) orientation, with highest orientation for the ITO films deposited at 150 °C. The lowest resistivity was $2.2 \times 10^{-3}$ Ω cm with a transmittance of about 85% in the visible region. With the increase of substrate temperatures, the crystalline quality of ITO films were improved possessing low microstrain, the Hall mobility increased to a maximum of 12.1 $cm^2$/V s, and the carrier concentration increased to a maximum of $3.4 \times 10^{20}$ $cm^{-3}$. The sheet resistance decreased to a minimum of 12.4 Ω/□ and the figure of merit reached a maximum for the ITO films deposited at 150 °C. The observation of relatively high band gap (3.58 eV), the optimum refractive index (1.95) and low extinction coefficient values in the visible region confirms the formation of highly crystalline, void free and compact ITO films at 150 °C. This is supported by the very low roughness values associated with the film surfaces as observed from the AFM pictures. These results reveal that a combination of high RF power (250 W) and moderate substrate temperature (150 °C) is capable of producing thermally stable and device quality ITO films with preferential orientation, lower resistivity and high transmittance.

## References


1. C.G. Granqvist, A. Hultaker, Thin Solid Films **411**, 1 (2002)
2. T. Minami, Semicond. Sci. Technol. **20**, 35 (2005)
3. D.S. Ginley, C. Bright, Mater. Res. Soc. Bull. **25**, 15 (2000)
4. G. Neri, A. Bonavita, G. Micali, G. Rizzo, N. Pinna, M. Niederberger, Thin Solid Films **515**, 8637 (2007)
5. H.L. Hartnagel, A.L. Dawar, A.K. Jain, C. Jagadish, *Semiconducting transparent thin films* (Institute of Physics, Bristol, 1995)
6. C.N. Carvalhio, A. Luis, O. Conde, E. Foitunato, G. Lavareda, A. Amaral, J. Non Cryst. Solids **299–302**, 1208 (2002)
7. A. ElHichou, A. Kachouane, J.L. Bubendroff, M. Addou, J. Ebothe, M. Troyon, A. Bougrine, Thin Solid Films **458**, 263 (2004)
8. V. Craciun, D. Craciun, X. Wang, T.J. Anderson, R.K. Singh, Thin Solid Films **453–454**, 256 (2004)
9. S. Kundu, P.K. Biswas, Chem. Phys. Lett. **414**, 107 (2005)
10. Z. Qiao, D. Mergel, Thin Solid Films **484**, 146 (2005)
11. H.R. Fallah, M. Ghasemi, A. Hassanzadeh, H. Steki, Mater. Res. Bull. **42**, 487 (2007)
12. S.H. Cho, J.H. Park, S.C. Lee, W.S. Cho, J.H. Lee, H.H. Yon, P.K. Song, J. Phys. Chem. Solids **69**, 1334 (2008)
13. Y. Abe, T. Nakayama, Mater. Lett. **61**, 3897 (2007)
14. J. Cui, A. Wang, N.L. Edleman, J. Ni, P. Lee, N.R. Amstrong, T.J. Marks, Adv. Mater. **13**, 1476 (2001)
15. N. Darson, I. Safi, G.W. Hall, R.P. Howsan, Surf. Coat. Technol. **99**, 147 (1998)
16. L.J. Meng, M.P. De Santos, Thin Solid Films **322**, 56 (1998)
17. H.C. Lee, O. Ok Park, Vacuum **80**, 880 (2006)
18. Y.S. Jung, S.S. Lee, J. Cryst. Growth **259**, 343 (2003)
19. S.I. Jun, T.E. Mcknight, M.L. Simpson, P.D. Rack, Thin Solid Films **476**, 59 (2005)
20. S. Mader, in *Handbook of thin film technology*, ed. by L.I. Maissel, R. Glang (Mcgraw Hill Book Company, New York, 1970), pp. 9–19
21. K. Ellmer, J. Phys. D Appl. Phys. **33**, R17 (2000)
22. E. Kubota, Y. Shigesato, M. Igarashi, T. Haranou, K. Suzuki, Jpn. J. Appl. Phys. **33**, 4997 (1994)
23. Powder diffraction file, Joint Committee on Powder diffraction Standards, ASTM
24. C. Kittel, *Introduction to solid state physics*, 5th edn. (Wiley, New York, 1976), p. 169
25. G. Frank, H. Kostlin, Appl. Phys. A **27**, 197 (1982)
26. C.H. Yi, I. Yasui, Y. Shigesato, Jpn. J. Appl. Phys. **34**, 1638 (1995)
27. D. Mergel, W. Stass, G. Ehl, D. Barthel, J. Appl. Phys. **88**, 2437 (2000)
28. M.-H. Yang, J.-C. Wen, K.-L. Chen, S.-Y. Chen, M.-S. Leu, Thin Solid Films **484**, 39 (2005)
29. C.V.R.V. Kumar, A. Mansingh, J. Appl. Phys. **65**(3), 1270 (1989)
30. E. Kubota, J. Shigesaato, M. Igarashi, T. Haranou, K. Suzuki, Jpn. J. Appl. Phys. **33**(Part 1 (9A)), 4997 (1994)
31. D.K. Shroder, *Semiconductor material and device characterization* (Wiley, New York, 1990)
32. J.I. Parkove, *Optical process in semiconductors* (Dover Publications, Inc., New York, 1971)
33. J. George, C.S. Menon, Surf. Coat. Technol. **132**, 45 (2000)
34. Y. Shigesato, S. Takaki, T. Haranoh, J. Appl. Phys. **71**, 3356 (1992)
35. J.C. Manifacier, J. Gasiot, J.P. Fillard, J. Phys. E **9**, 1002 (1976)

36. H.-N. Cui, V. Teixeira, A. Monterio, Vacuum **67**, 589 (2002)
37. S. Venkatachalam, D. Mangalaraj, D. Mangalaraj, Sa.K. Narayandass, Physica B **393**, 47 (2007)
38. A.N.H. Al-Ajit, S.C. Bayliss, Thin Solid Films **305**, 116 (1997)
39. C.H. Lee, C.S. Huang, Mater. Sci. Eng. B **22**, 223 (1994)
40. R. Das, K. Adhikary, S. Ray, Appl. Surf. Sci. **253**, 6068 (2007)
41. G. Haacke, J. Appl. Phys. **47**, 4086 (1976)
42. L. Zhao, Z. Zhou, H. Peng, R. Cui, Appl. Surf. Sci. **252**, 385 (2005)
43. Y.S. Kim, J.H. Park, D.H. Choi, H.S. Jang, J.H. Lee, H.J. Park, J.I. Choi, D.H. Ju, J.Y. Lee, D. Kim, Appl. Surf. Sci. **254**, 1524 (2007)
44. D. Kim, Opt. Mater. **24**, 471 (2003)